J Infrared Milli Terahz Waves (2016) 37:243–257
DOI 10.1007/s10762-015-0224-y

Room-Temperature AlGaN/GaN Terahertz Plasmonic Detectors with a Zero-Bias Grating

H. Spisser[1,3] · A.-S. Grimault-Jacquin[1] · N. Zerounian[1] · A. Aassime[1] · L. Cao[2] · F. Boone[3] · H. Maher[3] · Y. Cordier[4] · F. Aniel[1]

Received: 7 September 2015 / Accepted: 6 November 2015 /
Published online: 16 November 2015

Abstract In this paper, we present sensitivity measurement as well as measured and calculated absorption spectra for AlGaN/GaN THz plasmonic detector made of a metallic grating in-between two ohmic contacts. Detectors with different grating patterns have been fabricated and their sensitivity, reaching 1.9 μA/W at 77 K and 0.7 μA/W at 300 K, measured with a voltage applied between the ohmic contacts. It is the first time that such a detector shows THz detection with no voltage applied on the grating, namely with a bidimensional electron gas (2DEG) having a homogeneous electron density. These results are consistent with detection by drag-effect rectification. Measurements held between 0.648 and 0.690 THz show that the dependence of the sensitivity on the frequency follows the absorption spectrum, indicating that absorption is a crucial step in the detection process. Further simulations of absorption spectra show the tunability offered by such detector and allow us to predict frequency behavior for grating-biased detectors as well, in which the rectification is mainly governed by ratchet effect.

✉ H. Spisser
helene.spisser@u-psud.fr

1 Institut d'Electronique Fondamentale, Univ Paris Sud, CNRS, Universite Paris-Saclay, Bat. 220, rue Andre Ampere, Centre Scientifique d'Orsay, 91405 Orsay cedex, France

2 State Key Laboratory of Advanced Electromagnetic Engineering and Technology, Huazhong University of Science and Technology, Wuhan 430074, China

3 Institut Interdisciplinaire d'Innovation Technologique, Universite de Sherbrooke, Sherbrooke, J1K 0A5 Quebec, Canada

4 Centre de Recherche sur l'Hetero-Epitaxie et ses Applications, CNRS UPR-10, Valbonne 06560, France

Keywords Detector · Gallium nitride · Grating · Semiconductor device · Submillimeter wave device · THz device

1 Introduction

The terahertz (THz) frequency range presents a growing interest for many applications (biology, medicine, security, telecommunication...), involving a strong research effort to find compact, tunable, room-temperature operating and cheap sources, detectors and amplifiers, but also passive devices like waveguides [1–3]. The road of THz electronics was notably opened by the study of physics of plasma oscillations in low dimensional systems [4]. Since the early 2000s, field effect transistors (FETs), including high electron mobility transistors (HEMTs) based on III–V heterostructures [5], and Si-MOSFETs [6], have been studied for THz detection. Their responsivity has reached a few hundreds of V/W and noise equivalent power (NEP) of a few hundreds of pW/$\sqrt{\text{Hz}}$. On the other hand, devices have been specifically designed for THz detection. They include an antenna [7] or a grating [8] as coupling element, but up to now it is unclear if the basic physics in all kinds of these devices have the same nature. The highest sensitivities have been reached using an original asymmetric dual grating gate as presented in [9]. Namely, at room temperature, sensitivities of 22 kV/W have been obtained at 0.2 THz with an excellent NEP of 0.5 pW/$\sqrt{\text{Hz}}$ using an InAlAs/InGaAs/GaAs epitaxial structure [10] and 6 kV/W at 1.5 THz with a NEP of 60 pW/$\sqrt{\text{Hz}}$ using InAlAs/InGaAs/InP [11]. These state of the art plasmonic THz-detectors are composed of an asymmetric-dual-grating-gate, namely two interdigitated electrodes constituting a grating of asymmetric pattern, on top of a semiconductor heterostructure including a bidimensional electron gas (2DEG). Two ohmic contacts are set on either side of the grating to read out the DC response proportional to the incident power. The highest responsivity is obtained when one of the two interdigitated electrodes is set to a voltage close to the pinch-off, and a DC voltage is applied between the ohmic contacts. To our knowledge, detection using this type of devices on GaN has not been reported yet. However, THz detection using GaN HEMTs has already been measured [12, 13], showing a maximum sensitivity of 1.1 kV/W at 1 THz [14].

To study deeper the grating as coupling element, AlGaN/GaN heterostructures only covered by a metallic grating have been studied, showing plasmon-polariton (PP) resonances [1, 15–17]. These ones occur on absorption spectra when the two-dimensional longitudinal plasmon couples with incident THz wave.

Progress in study of the rectification reveals another way to develop highly sensitive non-cooled plasmonic THz detector. This rectification originates from the nonlinear behavior of the electron gas. In a basic modeling scheme, this nonlinear effect can be taken into account through the Euler equations and the conservation equation used to describe the 2DEG [16]. Two terms have been specially pointed out, namely the drag and ratchet effect [18]. The drag effect is greatly enhanced when a source-drain current is applied on the detector, leading to a break of the symmetry by the electric field [19]; thenceforth, the carrier density is spatially modulated through a

grating gate polarization, the ratchet effect joins the other nonlinear mechanisms [20]. Besides this, a second-order susceptibility of the quantum well could also participate in the rectification process operating on the photon diffracted by the grating.

The AlGaN/GaN heterostructure is particularly appropriate to study the rectification process as it allows one to have a homogeneous 2DEG under the metallic grating because of the coincidence of the metal-AlGaN Schottky barrier height and the Fermi level pinning under the slits of the grating. Furthermore, high N_s can be achieved in AlGaN/GaN without delta-doping because of the high electron concentration in the GaN near the AlGaN interface due to the electric field in the AlGaN barrier and the quantum well in GaN, both arising from the strong polarized wurtzite structure of the material [21, 22].

We present here sensitivity measurement of grated AlGaN/GaN THz plasmonic detectors as well as their measured and calculated absorption spectra. The structure of our devices and their fabrication process are detailed in Section 2, and the experimental results are presented in Section 3. In Section 4, simulated absorption spectra are presented for homogeneous and inhomogeneous electron sheet density below gratings with different types of pattern.

2 Description of the Detector and its Fabrication Process

The samples are based on AlGaN/GaN heterostructures on which, a Ti/Au grating between two ohmic contacts has been deposited (Fig. 1). The epitaxial structure consists of an AlGaN barrier layer above a GaN active layer grown on a sapphire substrate. The 2DEG has an electron sheet density (N_s) of $12 \times 10^{12}\,cm^{-2}$ at 300 K ($11 \times 10^{12} cm^{-2}$ at 77 K) and a mobility (μ) of $2100\,cm^2/Vs$ at 300 K ($9900\ cm^2/Vs$ at 77 K). These data have been extracted from Van der Pauw and Hall measurements. With a period P of 9.2 µm, the patterns of the gratings deposited on the detectors are composed of two metal bands of width L_1 and L_2 separated by slits of widths d_1 and d_2 (Fig. 1). The ratio $(L_1 + L_2)/P$ of the area covered by metal has been set at 75 %.

Once the heterostructure grown, a SiO_2 PECVD thin layer is deposited, followed by ohmic contacts using optical lithography. Afterwards, each device is isolated using crystal amorphization by ionic implantation. Finally, the grating has been deposited using e-beam lithography. The thickness of the gold grating is 400 nm in order to be larger than the THz skin depth. Processed by lift-off, this last fabrication step requires a quite high aspect ratio of very long resist ribbons with regard to slits having widths of hundreds of nanometer. Two kinds of samples are done: the first one has 6-mm ribbon length and the second one has 2-mm ribbon length. All samples are in agreement with the widths of the incident THz beams of different measurement setups. Figure 2 is a photograph of the sample and a scanning electron microscopy image (SEM) of one grating. Four detectors have been made in the sample with symmetric (numbered #1, #2) and asymmetric grating patterns (#3, # 4). Grating parameters are summed up in Table 1. The period of the grating has been chosen to exhibit a resonance at 0.65 THz at 300 K , which is the center frequency of the source

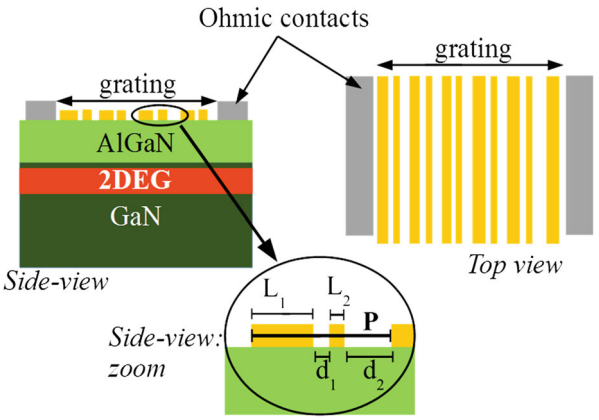

Fig. 1 Scheme of a typical detector. A gold grating is deposited in-between ohmic contacts on-top of an AlGaN/GaN heterostructure. We represented here an asymmetric pattern for the grating. For symmetric patterns $L_1 = L_2$ and $d_1 = d_2$

used here for the direct detection measurements. Grating dimensions were found by CST Microwave Studio modeling.

3 Measurements

In this section, we present the DC response to a THz radiation of plasmonic detectors with grating of symmetric and asymmetric patterns at room and cryogenic temperature, with and without bias voltage between the ohmic contacts, but keeping the grating unbiased. A study of the detector's response show higher responsivity and higher signal-to-noise ratio (SNR) at 77 K compared to 300 K, but no clear difference between symmetric and asymmetric patterns. This similarity between both types

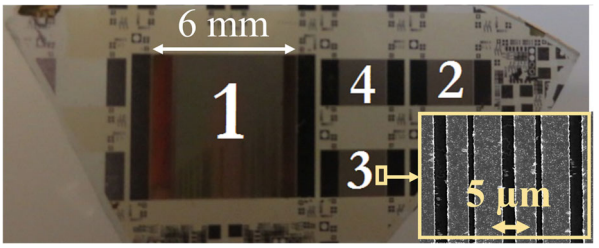

Fig. 2 Photograph of the processed sample and SEM image of the grating of detector #3. The numbers written on the photograph correspond to the detector numbers as indicated in Table 1

of patterns can be explained by the fact that the 2DEG under the grating is homogeneous in both cases. The study of the response with respect to the voltage applied between the ohmic contacts (V_{ds}) shows that the signal generated by the THz radiation and the noise increase with V_{ds}. The devices show then an optimal SNR for V_{ds} around 1.5 V. We obtained no measurable response when V_{ds} is zero. Measurements of sensitivity versus frequency show that the absorption is a crucial step of the detection since the frequency dependence of the sensitivity is similar to the one of the measured absorption.

3.1 Transmission and Reflection Spectra Measurements

Measurement of the absorption spectrum has been led using a Bruker 66v/S Fourier Transform Infrared Spectrometer (FTIR) to confirm the resonant frequency which should be close to 0.65 THz at 300 K and 0.60 THz at 77 K. The 7-GHz resolution of the FTIR can resolve the Fabry-Perot oscillations (period of 65 GHz) mainly caused by reflections in the sapphire substrate. This interference effect is suppressed from measurement spectra once averaged over the period of the Fabry-Perot oscillations. No bias voltage on the metallic strips of the grating nor between the two ohmic contacts is applied. The sample used for this measurement is the large detector #1 (see Table 1) to obtain high SNR and low diffraction effect. Its experimental spectra obtained at 77 K are shown in the inset Fig. 3. A resonance (a transmission valley and a reflection peak) occurs at 0.625 THz. Calculated spectra reported in Fig. 3 overlap the experimental data with a shift of 0.025 THz towards low frequencies. This discrepancy can result from imperfect devices in respect to modeling where the heterostructure (epitaxy) is idealized as the metallic grating dimensions. While the period is well defined the ribbons width suffer from lateral definition uncertainties induced by the thick resist lift-off process. Calculations with the ratio W / P diminished from 75 to 71.5 %, as measured on samples, show a resonant frequency of 0.612 THz, closer to experimental results.

The spectrum of the detector #1 allows to anticipate PP resonance for all detectors because the resonant frequency varies very slightly between the three different grating patterns (see Fig. 3). Results show that an asymmetric grating pattern [9] has a weak effect on the absorption, and its role is more crucial for rectification

Table 1 Grating parameters of the fabricated detectors

Detector	Grating area	L_1(μm)	L_2(μm)	d_1 (μm)	d_2 (μm)
1	6 mm × 6 mm	3.46	3.46	1.14	1.14
2	2 mm × 2 mm	3.46	3.46	1.14	1.14
3	2 mm × 2 mm	3.00	3.92	1.60	0.68
4	2 mm × 2 mm	2.78	4.14	1.82	0.46

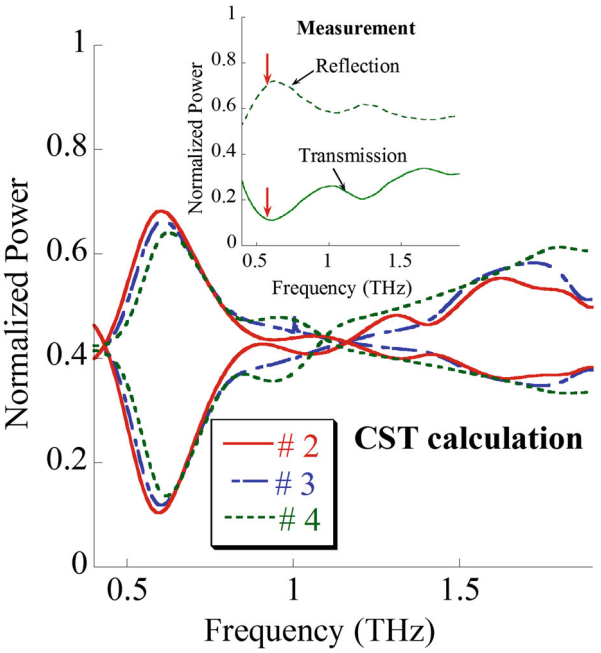

Fig. 3 Transmission and reflection spectra for the detector #2 (equivalent to detector #1), #3 and #4 calculated using CST at 77 K. The inset shows the spectra for the detector 1 measured by FTIR at 77 K. The curves have been smoothed to get rid of the Fabry-Perot oscillations in the substrate and the cryostat window. The *red arrows* in the inset indicate the calculated resonant frequency

phenomena. As a consequence, we lead sensitivity measurements around the absorption resonance in order to discriminate the nature of the rectification effect (drag or ratchet) operating in our configurations.

3.2 Detection Measurements

3.2.1 Description of the Experimental Bench

Measurements of the sensitivity for the detectors #2, #3, and #4 have been led at 300 and 77 K. The measurement setup is presented in Fig. 4: a continuous wave (CW) THz beam emitted from a Gunn oscillator-based frequency multiplied source is chopped and focused on the sample inside a cryostat. A bias voltage V_{ds} is applied between the ohmic contacts. The AC current is measured using either a lock-in amplifier or a Fast Fourier Transform (FFT) analyzer at the chosen chopper frequency (462 Hz).

The measured incident power (P_{in}) on the sample is maximum at 0.648 THz with 50 µW. Due to the CW source technology, this power cannot be constant with frequency. In some unfavorable case over the whole frequency range (from 0.6 to 0.72 THz), the maximum power can be divided by two. Although the resonance frequency is quite higher, because of the relatively high power, many measurements

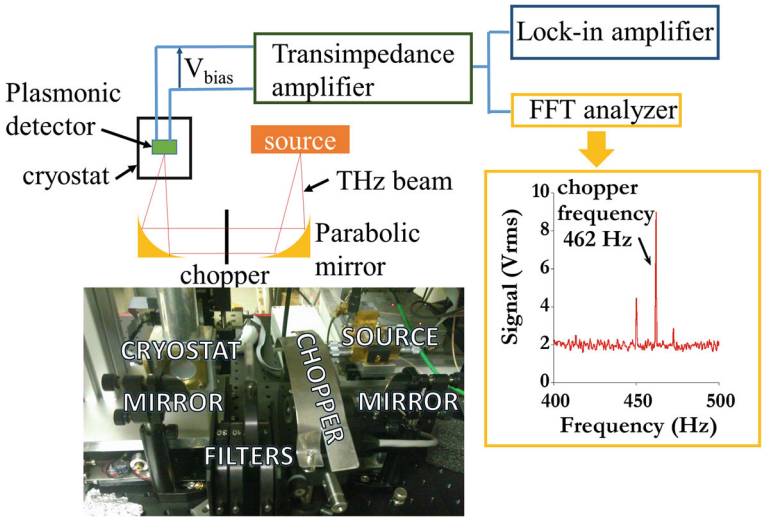

Fig. 4 Scheme and photo of the measurement setup used for the detection measurement. The curve in inset is a screen shot of the FFT analyzer

have been done at 0.648 THz. The influence of incident power and frequency and of bias voltage is analyzed on detection figures of merit such as the sensitivity, the photo-induced current, and the signal-to-noise ratio (SNR).

3.2.2 Influence of the Incident Power on the Detected Signal at 300 and 77 K

Using neutral filters placed just after the chopper, the maximum value of P_{in} is reduced by 50, 70, 90 and 100 %. It gives five measurements on each detector #2, #3, and #4 at 0.648 THz. The signal is deduced from the lock-in amplifier at the chopping frequency, and it is plotted in Fig. 5a, b at 300 and 77 K, respectively, with a V_{ds} bias of 1.5 V. The grating is unbiased.

The curves of the photo-induced current are firstly mingled with noise floor until a P_{in} threshold from where it increases linearly. The noise floors are indicated for each detector on the Fig. 5a, b. They are between 3 and 10 pA at 300 K and between 7 and 11 pA at 77 K. Using the sensitivity deduced a little further, noise floors can be converted into equivalent powers given in brackets in the graph, they range from 7 to 14 µW at 300 K. At 77 K, it is 6 µW for detectors #3 and #4, whereas it is 8 µW for the detector #2. Such a relative high noise floor comes from the small sensitivity, where any kind of perturbation (electrical, mechanical, and optical) is rapidly seen in high gain measurement chain. The sensitivity is deduced from the slope of the linear dependence of the detected signal with P_{in}, and it is weakly dependent on the geometry of the grating pattern. This linear power dependence is consistent with a second-order nonlinear effect where the response is proportional to the square of the electric field. At 300 K, the sensitivity varies from 0.4 µA/W for #2 to 0.7 µA/W for #3. A slightly better sensitivity is obtained for asymmetric detectors at room-temperature. At 77 K, the sensitivities of the three detectors are very close

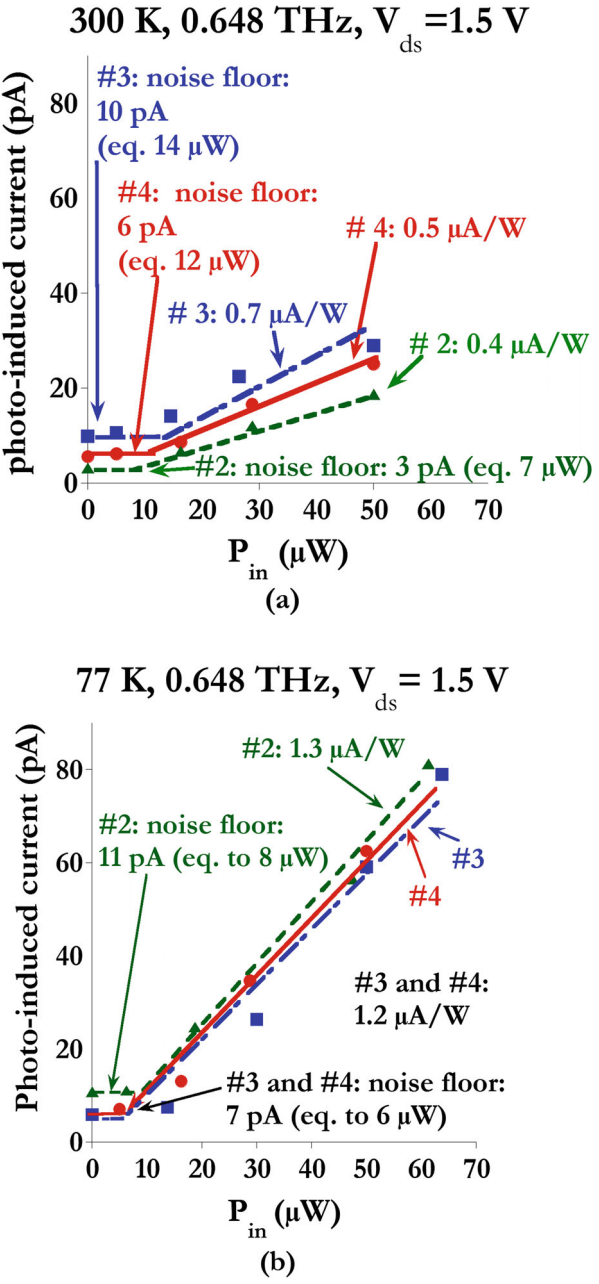

Fig. 5 Photo-induced current measured by the lock-in amplifier with respect to the incident power for detectors #2, #3, and #4 at 300 K (**a**) and 77 K (**b**) for a 0.648 THz incident radiation. A bias voltage of 1.5 V is applied. The *lines* stand for the noise floors and the linear fits. The sensitivity of each detector as well as its noise floor and equivalent noise floor power are indicated on the figure

one to another and reach 1.3 μA/W. The temperature dependence of the sensitivity is consistent with both drag and ratchet effects as described in [18]: an increase of the response is expected for lower electron scattering rates leading to a higher mobility at cryogenic temperature. The highest measured sensitivity is 1.9 μA/W for the detector #3 (asymmetric grating pattern) with V_{ds} of 1.75 V at 77 K. These sensitivity values are roughly seven orders of magnitude below the state of the art sensitivities achieved for grating-biased dual grating-gate detectors [10, 11]. This shows that the predominant rectification effect operating in THz plasmonic detectors as in [10, 11] is the ratchet effect, as it can only occurs when the 2DEG electron sheet density is periodically modulated. Indeed, the ratchet DC current arises as a result of the combined action of a static spatially periodic in-plane potential and the electric field of incoming radiation spatially modulated by a grating lattice [18]. It is the first time here that a signal is detected with unbiased grating and thus with homogeneous 2DEG, so that only the drag effect occurs consistently with [18].

3.2.3 Influence of the Bias Voltage on the Photo-Induced Current and SNR at 300 and 77 K

The normalized current and the SNR of the detector #3 are presented in function of the voltage bias V_{ds} at 300 and 77 K in Fig. 6. The signal-to-noise ratio (SNR) is calculated by dividing the current obtained with the incident power P_{in} of 50 μW at 0.648 THz by its noise floor obtained with a zero P_{in}.

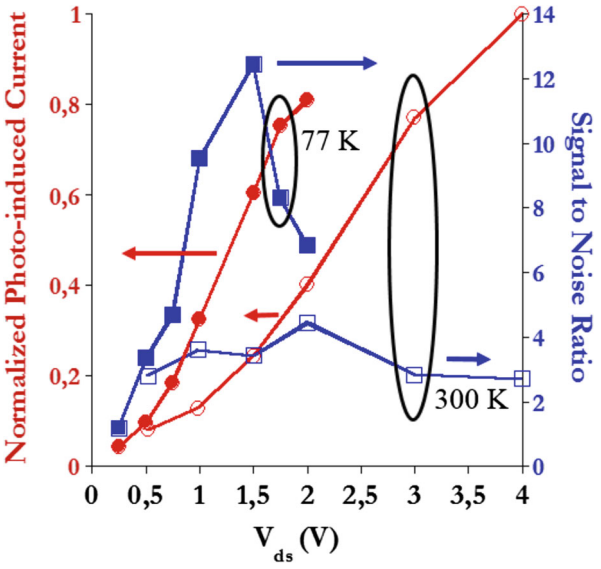

Fig. 6 Normalized photo-induced current and SNR with respect to the bias voltage for the detector #3 at 300 K (*open marks*) and 77 K (*solid marks*). The incident power is 50 μW at 0.648 THz

At 300 and 77 K, the photo-induced current increases with the applied voltage, but the noise also increases. The best SNR is obtained for $V_{ds} = 2$ V at 300 K and $V_{ds} = 1.25$ V at 77 K. The variation of photo-induced current and SNR with V_{ds} is similar for detectors #2 and #4. The increase of the photo-induced current can be explained using the theory developed in [19], where a maximum drag response is found for a drift velocity of electrons in the 2DEG equal to the plasmon velocity. For our detectors, the drift velocity (150 m/s with 1.5 V applied on 2-mm width device with an electron mobility of 2000 cm^2/Vs) is always well below the plasmon velocity (3×10^6 m/s for a wave at 0.648 THz with a wavelength of 4.7 µm), so the photo-induced current increases with the drift velocity set by the bias voltage V_{ds}. The drag effect discussed above originates from the nonlinear dynamics of electron in 2DEG described by hydrodynamic equations. The same hydrodynamic equations predict the existence of a ratchet effect when the electron sheet density in the 2DEG is periodically modulated [18]. In our case, the electron sheet density is homogeneous across the device, so this effect does not contribute to the rectification.

3.2.4 Comparison of FTIR and Detection Measurement Versus Frequency

The CW source is tunable between 0.6 and 0.72 THz, and it allows to measure the frequency dependence of the sensitivity around 0.648 THz for sample #2 with symmetric grating pattern. This measure is represented in Fig. 7 and compared with the absorption spectrum (FTIR) at 77 K of #1, with the same grating pattern.

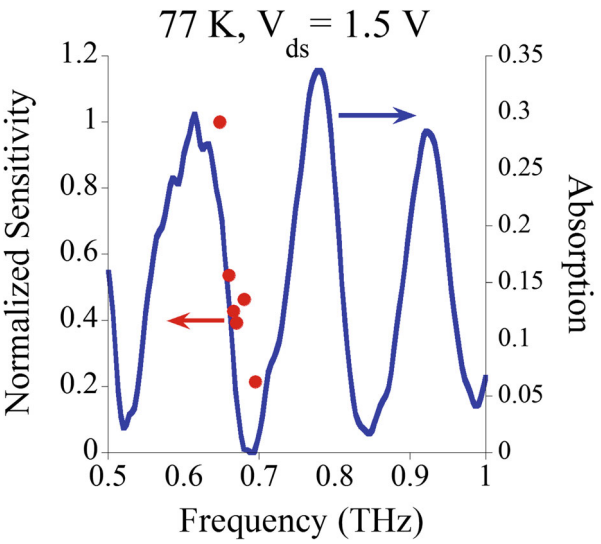

Fig. 7 Absorption spectrum measured by FTIR for the detector #1 at 77 K, without smoothing of the Fabry-Perot oscillations, and sensitivity measurement (*red points*) of the detector #2 versus frequency at 77 K for $V_{ds} = 1.5$ V. The sensitivity is normalized by its value at 0.648 THz. #1 and #2 have the same grating pattern and differ only by their area

The sensitivity measurements done between 0.648 and 0.690 THz show the same frequency dependence for the sensitivity and the absorption. A maximum occurs near the frequency where P_{in} is the highest and when it is located along a peak of the Fabry-Perot absorption oscillations. The similarity between the frequency dependence of the sensitivity and the absorption spectrum shows that the absorption is a crucial step in the detection process and a good indicator for the frequency dependence of the sensitivity. Our interest focuses on this point in the following section by means of complementary modeling.

4 Simulation Results

The measurement results have been completed by calculation of the absorption spectra for different configurations of the grating and spatial modulations of the electron sheet density using a commercial software and a homemade program. CST Microwave Studio have been used to model the absorption spectra of our AlGaN/GaN detector with symmetric ($L_1 = L_2$ and $d_1 = d_2$) and asymmetric ($L_1 \neq L_2$ and $d_1 \neq d_2$) grating pattern above a homogeneous 2DEG with various geometrical variations of grating dimensions to those studied experimentally. In a second time, the absorption spectra of symmetric grating patterns above an inhomogeneous 2DEG have been modeled with a homemade code based on the coupled wave method (CWM) using an expansion in spatial Fourier series of the inhomogeneous 2DEG permittivity [1]. Experimental data of our detectors, but much more the results reported in [10, 23], for dual grating-gate detectors, have shown that an asymmetric grating enhances the sensitivity of plasmonic detectors. First, the 2DEG is considered homogeneous as it is in our measurements. In a second time, through a simplified electromagnetic approach, some simulated results which treat the effect of the spatial modulation of the electron sheet density (N_s) on the absorption of grating-biased detector are presented; a full numerical investigation based on a 3D Maxwell Boltzmann solver [24] is under development. To lead numerical calculations, we refer to the nominal heterostructure as the one described in Section 2. The 2DEG is modeled as a 12-nm-thick layer with an anisotropic permittivity (dispersive and adapted from the Drude model [1] in the 2DEG plane, and equal to 9.7 ϵ_0 normal to the plane,where ϵ_0 is the vacuum permittivity). In this last case, the permittivity of the 2DEG layer is different under the metal bands and under the slits where two different N_s have been fixed. The grating is considered as infinite using periodic boundary conditions in the plane of the grating and perfect matched layer boundaries in the direction of propagation of the incident THz radiation. Different values of the grating period and percentage of metal coverage have been investigated.

4.1 Absorption Spectra of a Homogeneous 2DEG Under Symmetric and Asymmetric Grating Patterns

This section deals with the influence of the grating geometry (symmetric or asymmetric) and period on the first (more intense in amplitude) PP resonance defined from the absorption spectra. It should be noticed that the analysis of this work is obtained from

the treatment of multiple simulations from CST (more than 50 different structures studied). Knowing that PP resonances of each structure converge to a same tendency versus grating period, only a little bit more than a dozen of points have been selected and reported on Fig. 8.

As observed in Fig. 8, the frequency of the first PP resonance decreases when the grating period rises up. For instance, for a period of 5 µm, the PP resonance appears at 0.5 THz whereas for a period of 1 µm, the resonance is at 2 THz. Micrometer size period variations can tune the resonance in a wide frequency range from hundreds of gigahertz to at least 3 THz. Asymmetric grating results are similar to symmetric ones. When no bias is applied neither to ohmic contacts nor to the grating, the asymmetry plays a minor or no role on the tunability of the PP resonance. Since the period dependence of the resonance frequency is preserved, the heterostructure with a symmetric grating can assess the position of the first resonance peak of all symmetric and asymmetric grating pattern structures. This is in agreement with experimental results of the Section 3.2.2, where the asymmetry has a very low influence on the detection sensitivity. This makes us briefly assume that when a strengthening of the rectification mechanisms is envisaged by making the grating asymmetric, the PP coupling is globally preserved since the first PP resonance frequency does not fluctuate.

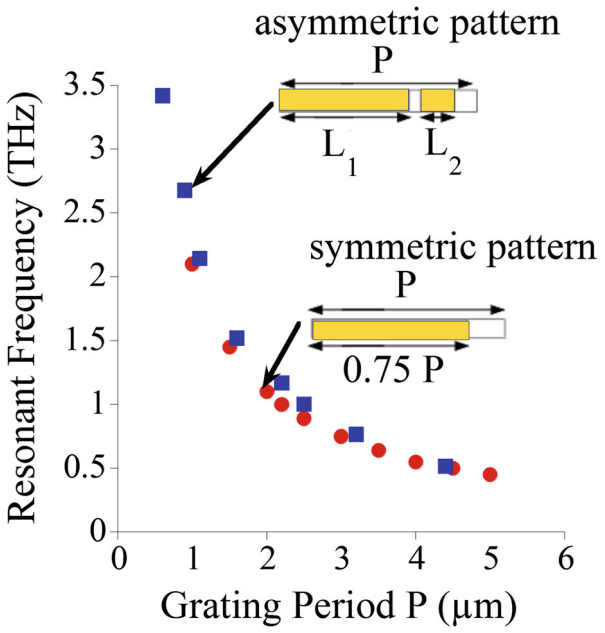

Fig. 8 Dependence of the first resonant frequency with the grating period for a symmetric (*red circles*) and for an asymmetric (*blue squares*) pattern. The dimensions of the asymmetric pattern are $L_1 / L_2 = 4$, $d_1 / d_2 = 2$ and $(L_1 + L_2) / P = 0.75$

4.2 Absorption Spectra of an Inhomogeneous 2DEG Under a Symmetric-Pattern Grating

The expression of the galvanoplasmonic current density shows that the rectification is essentially controlled by the electron density in the 2DEG [25]. As already done on AlGaAs/GaAs [1], we can modify the nominal resonant absorption by modulating the electron density using a grating voltage. When applying a bias voltage V_g on the grating, N_1, the electron sheet density below the metal fingers (see inset Fig. 9) will be modified, inducing a change in the absorption spectra of the device. In this study, we keep N_2 constant while we modulate N_1 between 12×10^{12} cm^{-2} and 3×10^{12}cm^{-2}

The tunability of PP resonances can be obtained by varying the electron density (namely V_g). When N_1 decreases (as V_g), the absorption is reduced also. For $N_1 = 3 \times 10^{12}$cm^{-2} ($N_2 = 12 \times 10^{12}$cm^{-2}), three resonances appear with an amplitude close to each other and it becomes less easy to separate them. The resonances tend to broaden and to shift to higher frequencies, and the amplitude can decrease by 30 %. When N_1 is low enough, the frequency bandwidth where the rectification can occur can be widespread by several terahertz, giving a flatter response of the PP absorption. These simulations show as well that one must be very careful while interpreting results obtained with a biased grating as the absorption spectra can

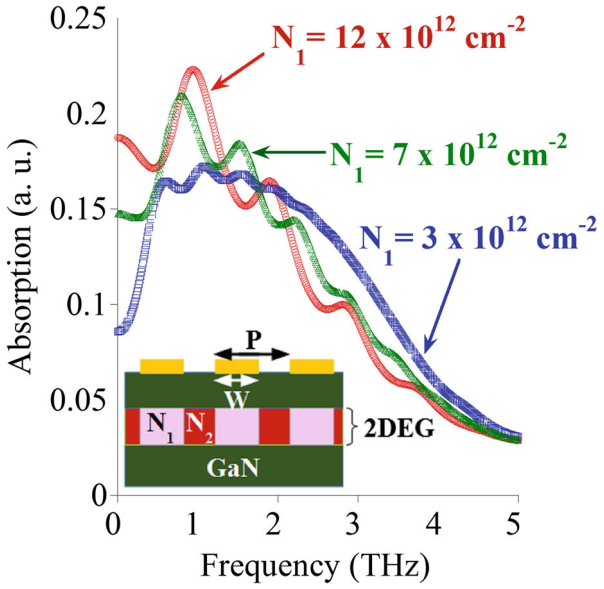

Fig. 9 Absorption spectra calculated with the coupled wave method for different N_1, the sheet carrier density below the grating finger. The sheet carrier density below the slits (N_2) is kept at 12×10^{12} cm^{-2}. The period of the grating P is 2.2 µm and the metal filling factor W/P is 0.75

be quite different depending on the grating voltage and because different nonlinear mechanisms can occur simultaneously.

5 Conclusion

By its experimental and numerical aspects, this paper opens a road for a pragmatic optimization of THz plasmonic detectors based on AlGaN/GaN heterostructure covered by a metallic grating. We focus on detectors with unbiased grating, having a homogeneous electron sheet density, and we present the first THz detection measurement in this configuration. Our experimental results show the necessity of applying a voltage between the ohmic contacts for an unbiased grating. This voltage enhances the photo-induced response, in agreement with a rectification by drag effect [19], but raises the noise floor as well. The comparison of the frequency dependence of the sensitivity and the absorption spectrum show the importance of the photon-plasmon coupling in the detection process. Simulations focusing on this coupling show the double tunability of such detector: by the grating period and by the grating bias. Both simulations and experiments show no large difference between detectors with symmetric and asymmetric grating patterns, unlike what happens with biased grating, for which asymmetric patterns enhance the sensitivity [23]. In future works, it will be interesting to polarize the grating to achieve a higher sensitivity and to study the relative importance of the drag and ratchet effects, as the later one only occurs in a 2DEG with a periodically modulated electron density. This will also be completed by a full numerical calculation based on a Maxwell Boltzmann solver [24] under development.

Acknowledgments The authors acknowledge the support from GANEX (ANR-11-LABX-0014). GANEX belongs to the public funded Investissements d'Avenir program managed by the French ANR agency. This work was partly supported by the French RENATECH network.

References

1. L. Cao, A.-S. Grimault-Jacquin, F. Aniel, Applied Physics A, 109 (4), 985 (2012).
2. L. Cao, A.S. Grimault-Jacquin, N. Zerounian, F. Aniel, Infrared Physics and Technology 63, 157 (2014).
3. A. Malekabadi, S. Charlebois, D. Deslandes, F. Boone, S. Member, IEEE Transactions on Terahertz Science and Technology 4(4), 447 (2014).
4. M. Dyakonov, M. Shur, S. Petersburg, Physical Review Letters 71(15), 2465 (1993).
5. J.Q. Lu, M. Shur, J. Hesler, R. Weikle, IEEE Electron Device Letters 19(10), 373 (1998).
6. W. Knap, F. Teppe, Y. Meziani, N. Dyakonova, J. Lusakowski, F. Boeuf, T. Skotnicki, D. Maude, S. Rumyantsev, M.S. Shur, Applied Physics Letters 85(4), 675 (2004).
7. A. Di Gaspare, R. Casini, V. Foglietti, V. Giliberti, E. Giovine, M. Ortolani, Applied Physics Letters 100(20), 203504 (2012).
8. X.G. Peralta, S.J. Allen, M.C.Wanke, N.E. Harff, J.a. Simmons, M.P. Lilly, J.L. Reno, P.J. Burke, J.P. Eisenstein, Applied Physics Letters 81(9), 1627 (2002).
9. D. Coquillat, S. Nadar, F. Teppe, N. Dyakonova, S. Boubanga-Tombet,W. Knap, T. Nishimura, T. Otsuji, Y.M. Meziani, G.M. Tsymbalov, V.V. Popov, Optics express 18(6), 6024 (2010).
10. Y. Kurita, G. Ducournau, D. Coquillat, A. Satou, K. Kobayashi, S. Boubanga Tombet, Y.M. Meziani, V.V. Popov, W. Knap, T. Suemitsu, T. Otsuji, Applied Physics Letters 104(25), 251114 (2014).

11. S. Boubanga-Tombet, Y. Tanimoto, A. Satou, T. Suemitsu, Y.Wang, H. Minamide, H. Ito, D.V. Fateev, V.V. Popov, T. Otsuji, Applied Physics Letters 262104, 1 (2014).
12. W. Knap, V. Kachorovskii, Y. Deng, S. Rumyantsev, J.Q. Lu, R. Gaska, M.S. Shur, G. Simin, X. Hu, M.A. Khan, C.a. Saylor, L.C. Brunel, Journal of Applied Physics 91(11), 9346 (2002).
13. J.D. Sun, H. Qin, R.A. Lewis, X.X. Yang, Y.F. Sun, Z.P. Zhang, X.X. Li, X.Y. Zhang, Y. Cai, D.M. Wu, B.S. Zhang, aplied physics letters 106, 031119 (2015).
14. T. Tanigawa, T. Onishi, S. Takigawa, T. Otsuje, S. Company, P. Corporation, T. Tanaka, in device research conference, vol. 024519 (IEEE, south bend, IN, 2010), vol. 024519, pp. 167168 (2010).
15. A.V. Muravjov, D.B. Veksler, V.V. Popov, O.V. Polischuk, N. Pala, X. Hu, R. Gaska, H. Saxena, R.E. Peale, M.S. Shur, Applied Physics Letters 96(4), 042105 (2010).
16. (V.V. Popov, Journal of Infrared, Millimeter, and Terahertz Waves 32(10), 1178 (2011)).
17. H. Spisser, A.S. Grimault-Jacquin, N. Zerounian, A. Aassime, L. Cao, F. Boone, H. Maher, Y. Cordier, F. Aniel, in Global Symposium on Millimeter-Waves, Montreal (2015).
18. V.V. Popov, Applied Physics Letters 102(25), 253504 (2013).
19. G.R. Aizin, V.V. Popov, O.V. Polischuk, Applied Physics Letters 89(14), 143512 (2006).
20. I. Rozhansky, V. Kachorovskii, M. Shur, Physical Review Letters 114(24), 246601 (2015).
21. O. Ambacher, B. Foutz, J. Smart, J.R. Shealy, N.G. Weimann, K. Chu, M. Murphy, a.J. Sierakowski, W.J. Schaff, L.F. Eastman, R. Dimitrov, A. Mitchell, M. Stutzmann, Journal of Applied Physics 87(1), 334 (2000).
22. X.G. He, D.G. Zhao, D.S. Jiang, Chinese Physics B 24(6), 067301 (2015).
23. T. Watanabe, S.A. Boubanga-tombet, Y. Tanimoto, D. Fateev, V. Popov, D. Coquillat, W. Knap, Y.M. Meziani, Y. Wang, H. Minamide, IEEE sensors journsl 13(1), 89 (2013).
24. M. Sirbu, S.B.P. Lepaul, F. Aniel, IEEE Transactions on Microwave Theory and Techniques 53(9), 2991 (2005).
25. D.V. Fateev, V.V. Popov, T. Otsuji, Y.M. Meziani, in Metamaterials, 1, pp. 532534 (2012).